Influence of the environment on the Coulomb blockade in submicrometer normal-metal tunnel junctions

A. N. Cleland, J. M. Schmidt, and John Clarke
Department of Physics, University of California, Berkeley, Berkeley, California 94720
and Materials Sciences Division, Lawrence Berkeley Laboratory, Berkeley, California 94720
(Received 22 August 1991)

Submicrometer normal-metal tunnel junctions were fabricated with thin-film leads of either about 2 $k\Omega/\mu m$ or about 30 $k\Omega/\mu m$. The current-voltage (I-V) characteristics at millikelvin temperatures displayed a much sharper Coulomb blockade for the high-resistance leads than for the low-resistance leads. The zero-bias differential resistance increased as the temperature was lowered, flattening off at the lowest temperatures. A heuristic model based on the quantum Langevin equation is developed, which explains these effects qualitatively in terms of the Nyquist noise generated in the leads; in this model, the flattening of the zero-bias resistance arises from zero-point fluctuations. The data are also compared with a more accurate phase-correlation model that treats the junction and the circuit coupled to it as a single quantum circuit. This model accounts for the observed I-V characteristics quite accurately except near zero bias where it overestimates the dynamic resistance by roughly 50% at the lowest temperatures. This model, however, does not account for the flattening of the zero-bias resistance at the lowest temperatures. It is suggested that the addition of quantum fluctuations in the junction to the phase-correlation theory may account for this discrepancy.

I. INTRODUCTION

Over the past few years there has been a large theoretical and experimental effort to understand the behavior of normal-metal tunnel junctions in the limit where the junction capacitance becomes very small.[1] The inclusion of a term in the Hamiltonian which transfers single electrons introduces additional features in the I-V characteristics of these junctions. One prediction is the appearance at zero temperature of a region of voltage $-e/2C < V < e/2C$ where no tunneling occurs. At any nonzero temperature $T < e^2/2k_BC$ the tunneling rate is exponentially suppressed below that expected from the tunneling resistance. This voltage regime, called the Coulomb blockade region, appears because of the single-electron nature of tunneling: the energy of charging the capacitance C of a small junction to a charge Q is $E_Q = Q^2/2C$, whereas after an electron has tunneled, the energy is $E'_Q = (Q-e)^2/2C$, where $-e$ is the electron charge. The energy change $\Delta E = E'_Q - E_Q$ is positive for $|Q| < e/2$, and negative for $|Q| > e/2$. The additional energy required for an electron to tunnel for $|Q| < e/2$ can be supplied only by a temperature bath, so that, at low enough temperatures, tunneling is energetically unfavorable. For voltages $V = Q/C$ in the Coulomb blockade region, tunneling will therefore not occur. Using electron-beam lithographic technology, one can fabricate tunnel junctions with geometric capacitances of the order of 10^{-15} F, corresponding to the appearance of a Coulomb blockade for $T \lesssim 1$ K. A number of experiments have been performed to investigate this phenomenon,[2-6] with most of them concentrating on multiple junctions connected in series; in general, single junctions did not behave in the manner predicted, and the Coulomb blockade was visible in the current-voltage (I-V) characteristic only as an offset at very large bias currents. There were also indications from the multiple-junction experiments that the single junctions were strongly affected by the external circuit. The multiple-junction experiments of Delsing *et al.*[4,5] and Geerligs *et al.*[6] were interpreted as a single junction isolated from its external environment by the other junctions, although this picture is not clear from microscopic considerations since the multiple junctions clearly constitute a more complex system.

The experimental and theoretical work described here was intended to observe the Coulomb blockade in a single small-capacitance tunnel junction, and to provide a simple explanation for the behavior seen in these and other single-junction experiments. The basic idea behind these experiments was to attempt to isolate the small junction from the leads connected to it by means of thin-film resistors in series with the junctions. We designed these thin-film resistors to operate at high enough frequencies and to have high enough resistance that they could significantly affect the dynamic behavior of the junctions. In the following sections, we describe the design of the small junctions and the resistors connected to them. We then present measurements of the I-V characteristics and the differential resistance as functions of temperature. These data show quite clearly that, for low-resistance leads, the Coulomb blockade is very smeared out, while for higher-resistance leads the blockade is much more sharply defined. We then describe two theoretical approaches to explain these data. The first is a heuristic model based on the quantum Langevin equation and appears to explain the general features. The second, which we refer to as the phase-correlation theory,[7-9] will then be outlined and its predictions compared with the data. Finally, we discuss the possible effects of finite junction-

 ©1992 The American Physical Society

tunnel resistance. A brief report of this work has appeared elsewhere.[10]

II. EXPERIMENTAL DESIGN

A. Thin-film resistors—RC transmission line model

The early theories predicting the appearance of the Coulomb blockade in a single, small tunnel junction implicitly assumed that the junction is isolated from the external environment. In any actual measurement, however, the wires attached to the junction electrodes necessarily introduce large stray capacitances, and unavoidably present a high-frequency impedance of order 10^2 to 10^3 Ω at the relevant characteristic frequencies. The presence of this large stray capacitance and small impedance is likely to affect the small junctions strongly, and most certainly has great influence on the behavior seen in the multiple- and single-junction experiments discussed above.

To minimize the effects of the stray capacitance and the low impedance leads, we designed the layout of the junctions to include thin-film resistors on the chip. In the ideal case, an infinite resistance at all relevant frequencies inserted between the small junction and the rest of the circuit isolates the junction, as it then takes an infinite time to resupply the junction with charge from the external leads. In the absence of such idealized leads, theoretical calculations indicate that a shunt resistor must be larger than the quantum of resistance $R_K/4=h/4e^2=6.45$ kΩ for the electrons to be well localized on either side of the junction;[11] the leads must therefore have a total resistance of at least 6.45 kΩ.

One can model the electrical impedance $Z(\omega)$ at frequency ω presented by a straight resistive lead typical of those used in these experiments fairly easily; a metal strip of length Λ and cross-sectional area A has a resistance R_L, a self-capacitance C_L, and a self-inductance L_L, all of which can be calculated from geometric considerations. One finds $R_L=\rho\Lambda/A$, where ρ is the resistivity, $C_L\approx(9.8f$ F/mm)Λ (assuming the resistor is fabricated on a SiO_2 substrate),[12] and $L_L\approx(1$ nH/mm)Λ.[13] These distributed elements from a resistive transmission line of impedance $Z(\omega)\approx R_L$ for frequencies $\omega\ll 1/R_LC_L$ and $Z(\omega)\approx\sqrt{R_L/\omega C_L}(1-i)$ for $\omega\gg 1/R_LC_L$. Given these considerations, we see one can achieve the highest values of $Z(\omega)$ while keeping the stray capacitance at a minimum by using a high-resistivity material with as small a cross-sectional area as possible.

B. Hot-electron effect

The difficulty one encounters when reducing the cross-sectional area of a resistive lead is that hot-electron effects become very important. Electrons lose energy by emitting phonons into the environment, and, for electrons at a temperature T_e, the characteristic frequency of the emitted phonons is $\omega_{ph}=k_BT_e/\hbar$. For very low temperatures T_e, the available phonon phase space is proportional to ω_{ph}^3, the electron-phonon coupling constant is proportional to ω_{ph} (in the deformation potential approximation), and the energy of the typical emitted phonon is proportional to ω_{ph}. As a result, the electron energy emission rate is proportional to ω_{ph}^5, and the electrons and phonons fall out of thermal equilibrium at low temperatures. The electron and phonon gases are then described by different temperatures T_e and T_{ph}, respectively. If power P is dissipated by Ohmic losses when a bias current I passes through the resistive leads, the electron and phonon temperatures T_e and T_{ph} in the resistive leads satisfy[14]

$$\frac{P}{A\Lambda}=\frac{I^2\rho}{A^2}=(2\times10^9\ \mathrm{W/m^3\,K^5})(T_e^5-T_{ph}^5)\ . \quad (1)$$

Clearly the resistivity ρ should be minimized and the cross-sectional area A maximized to reduce the electron heating. Unfortunately , this is in direct conflict with our need for high impedances at high frequencies.

C. Resistor design and fabrication techniques

In the final design of the resistive leads we attempted to reduce the heating while maintaining a high impedance to as high a frequency as possible. For our first resistor design, we chose an alloy of Au (25 wt. % Cu) for its reliability and ease of fabrication. A thickness of 30 nm produced a continuous film with resistivity 12 μΩ cm. Using Eq. (1), we find that, for this resistivity and film thickness, a 2-μm-wide resistor should not be heated appreciably by a typical bias current of a few nA (see Fig. 1). To achieve a minimum zero-frequency lead resistance of 60 kΩ [so that $R_L\approx10(R_K/4)$], we were forced to include a large number of meanders on each lead (see Fig. 2). Each meander capacitively couples across itself, and we chose the spacing and length of each meander so that this cou-

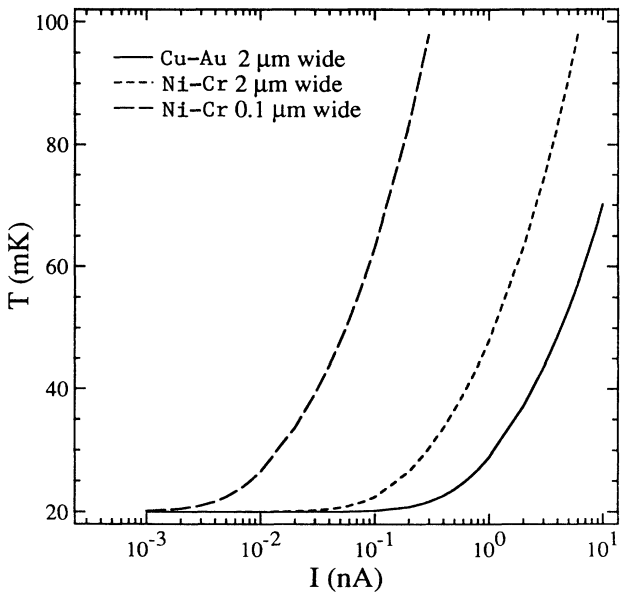

FIG. 1. Calculated dependence of electronic temperature T_e on bias current I, for 30-nm-thick and 2-μm-wide Cu-Au, for 30-nm-thick and 2-μm-wide Ni-Cr, and for 30-nm-thick and 0.1-μm-wide Ni-Cr. The calculations assume a phonon temperature $T_{ph}=20$ mK.

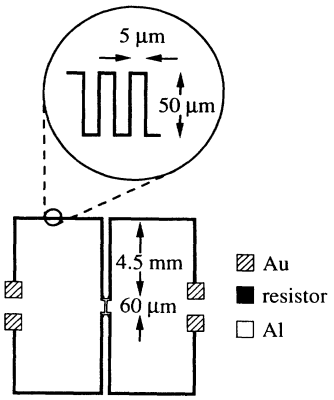

FIG. 2. Layout for the small junction measurements. The Cu-Au leads meandered after the first 4.5 mm leading out from the junction (shown in the inset); the Ni-Cr leads were straight.

pling would begin to roll off the impedance only above 10^{10} Hz. We ignored the self-capacitance of the leads. Thus, the first design involved two, 2-μm-wide lines coming straight out of each lead of the junction, extending 4.5 mm to near the edge of the chip, and then following a 2-μm-linewidth meander around the perimeter of the chip to the four 0.5 mm$\times$0.5 mm contact pads. We subsequently realized that the self-capacitance of the 2-μm leads was sufficient to effectively short out all but the first few millimeters of the leads above about 10^8 Hz. Thus, the meanders did not provide any significant resistance above that frequency and were replaced by straight lines to the contact pads in the second resistor design. The lines were made of 2-μm-wide Ni (30 wt.% Cr) films 25–30 nm thick with a resistivity of 120 $\mu\Omega$ cm (see Fig. 2). Although not as effective as the Cu-Au resistors for eliminating heating effects, Ni-Cr resistors of this width also should not cause a problem for low bias currents (see Fig. 1). For completeness we also show the electronic temperature versus bias current for a 0.1 μm-wide Ni-Cr resistor and note that heating can be significant.

To fabricate the samples, we used a combination of optical and scanning electron microscope (SEM) lithography. All the samples were made on Si wafers 50 mm in diameter, with a 1000-nm-thick SiO_2 insulating layer. The SEM lithography followed published recipes, with a suspended resist bridge made with a bilayer of PMMA and a copolymer, P(MMA-MAA).[15,16] The junctions were fabricated from Al with a standard angle evaporation technique.

We used evaporated Au pads as a contact surface both for the Al that made up the junctions and for external electrical lead connections. A Cr underlayer 2–3 nm thick was evaporated first to ensure adhesion of the Au layer. Both the Cu-Au and Ni-Cr resistors were deposited by evaporation; the Cu-Au was preceded by a Cr underlayer 2–3 nm thick. The evaporation of Ni-Cr from a length of wire is a technique suggested by Martinis and Kautz.[17]

To fabricate the Al tunnel junctions, we first evaporated a Cu layer, about 5 nm thick, to ensure good electrical contact between the Al and the Au contact pads at the ends of the resistive leads. The Cu film contacted the Al only at the Au contact pads and was at least 200 nm from the junction itself. We then evaporated the Al to a thickness of about 40 nm with a relatively high evaporation rate, 5–10 nm/sec, to prevent the Al from oxidizing. We oxidized the Al in about 0.5 Torr of 30 mol.% O_2+Ar for 10 min, and then deposited the second 40-nm-thick Al film. We lifted off the Al in boiling acetone. Typical junction areas were about 0.02 μm^2, and the contacts to the Au pads at the end of each of the 40-μm-long Al leads were about 10 μm^2.

D. Refrigerator design, wiring, and measurements

The sample mount consisted of a Cu plate bolted to a Cu rod which screwed into the mixing chamber of a dilution refrigerator. A rectangle of G-10 fiberglass was glued to the plate with Stycast 2850 epoxy, and a glass slide was, in turn, glued to the fiberglass with the same epoxy. The Si chip with the junction was attached to the glass slide with vacuum grease and was at least 8 mm from any metal surfaces. The Al junctions were driven into the normal state by two Nd-Fe-B permanent magnets, mounted in a steel yoke, that produced 1100 Oe at the chip (see Fig. 3). We used In to cold weld the four current and voltage leads to the Au contact pads on the chip. Each lead passed through a block of stainless-steel powder (with a grain size of about 50 μm) mixed with Stycast 2850 epoxy; this structure formed a microwave filter with at least 10 dB of attenuation above 1 GHz (see Fig. 3).[18] The leads, junction, and steel powder block were surrounded by a Cu radiation shield. Further filtering of each lead was provided at 4.2 K by filters potted in stainless-steel powder and epoxy, with a 3-dB rolloff point at 16 kHz, and at room temperature by a radiofrequency filter, with 120 dB of attenuation above 100 MHz (see Fig. 4).

Our current supply consisted of a voltage source in series with a 50-MΩ resistor, a 2-MΩ resistor to measure the current, and a low-pass RC filter with a rolloff frequency adjustable to between 3 and 100 Hz. A low-noise amplifier was connected across the voltage leads. The

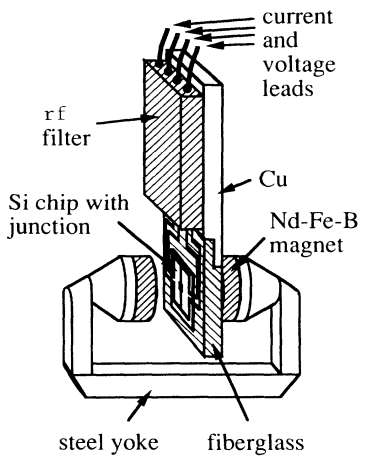

FIG. 3. Sketch of junction mount.

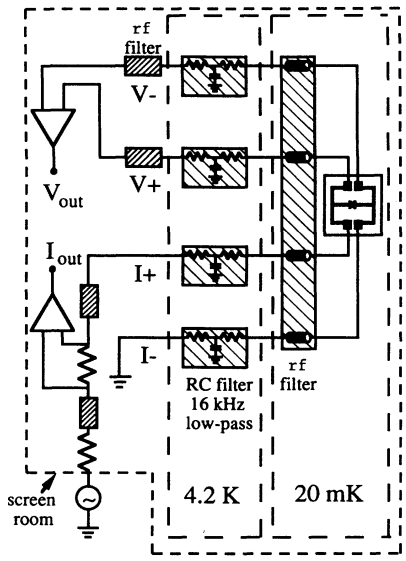

FIG. 4. Wiring schematic for dilution refrigerator.

amplifiers were battery powered and, together with the current supply, were inside the screened room. No line power was brought into the screen room during the measurements.

We recorded I-V traces on an analog X-Y plotter, and obtained I versus dV/dI traces using a lock-in technique with a very low-frequency sweep for the current (typically 1–3 mHz), and a 15–20-Hz current modulation for the lock-in measurement. The modulation amplitude was typically 1% of the full sweep amplitude: for example, for a 1-nA sweep we used a 10-pA peak-to-peak modulation current. The alternating voltage was lock-in detected, and the traces were recorded on an X-Y plotter. Reducing the modulation amplitude by a factor of 5 had no effect on the traces. We calibrated the differential resistance by comparing it with an I-V trace.

The two largest sources of spurious noise were 60-Hz pickup and vibrational noise, the latter presumably induced by wires moving relative to ground. We reduced the 60-Hz pickup to about 20 nV peak-to-peak across each pair of leads by very carefully isolating the screened room from all grounds. A μ-metal shield was placed around the lower part of the refrigerator, at the height of the sample. A second μ-metal shield could either be placed concentrically to the first shield, or placed around a platform which held the amplifiers and the current-limiting resistors forming a small magnetic and electric screened room, internal to the Cu-mesh screen room.

III. EXPERIMENTAL RESULTS

A. I-V characteristics and dV/dI measurements

We fabricated and measured nine small junctions. In Fig. 5, we show the I-V characteristics at 20 mK of two typical junctions, one with Cu-Au leads with a lead resistance of 2 kΩ/μm (junction 5 in Table I), and the other with Ni-Cr leads with a resistance of 30 kΩ/μm (junction

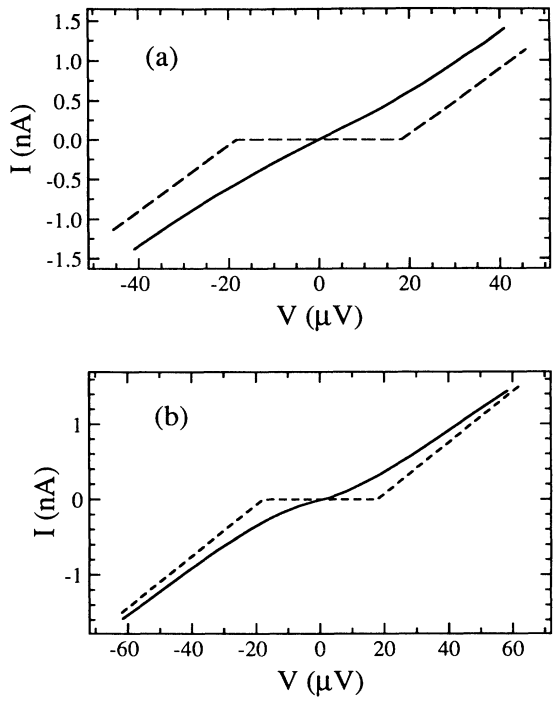

FIG. 5. I-V characteristics (solid lines) measured for two small junctions at $T=20$ mK. (a) Junction 5 with Cu-Au leads, $R_J=23$ kΩ, and $C_J=4\pm1$ fF. (b) Junction 7 with Ni-Cr leads, $R_J=29.4$ kΩ, and $C_J=5\pm1$ fF. Dotted lines show predicted voltage-biased Coulomb blockade for each junction.

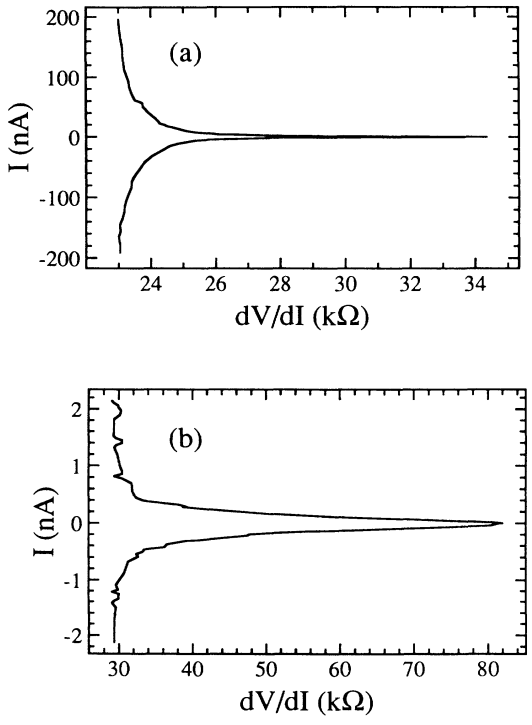

FIG. 6. Measured dV/dI at 20 mK (a) junction 5 and (b) junction 7; note the difference in current scales.

TABLE I. Summary of experimental parameters. R_J is the tunneling resistance (measured at high bias), C_J the junction capacitance inferred from the high-bias voltage offset, ZBR the zero-bias resistance at $T=20$ mK, and R_L the resistance of one lead to the junction. Lead material is given in the last column.

Junction	R_J (kΩ)	C_J (fF)	ZBR (kΩ)	R_L (kΩ)	Lead material
1	6.0	3±0.5	6.9	132	Cu-Au
2	32.2	12[a]	44	140	Cu-Au
3	11.3	3±1	14.8	162	Cu-Au
4	27	3±1	39.5	92	Cu-Au
5	23	4±1	34.3	150	Cu-Au
6	8.8	6.5±1	18.4	390	Ni-Cr
7	29.4	5±1	82	350	Ni-Cr
8	133	3±1	464	350	Ni-Cr
9	82	3.5±1	239	340	Ni-Cr

[a]Only a small I_{bias} is used, hence C is probably overestimated.

7 in Table I). The dotted lines show the voltage-biased Coulomb blockade characteristic expected at $T=0$. It is clear that the Coulomb blockade is only barely visible in junction 5, while it is quite sharply defined in junction 7. Figure 6 shows the differential resistance; it is clear that for junction 5 one must apply about 100 nA of bias current before the differential resistance approaches its asymptotic value R_J, while for junction 7 one only need apply about 1 nA. The lead resistance clearly affects the I-V characteristic profoundly. In Fig. 7 we plot the zero-bias resistance (ZBR) of seven junctions, normalized to R_J, as a function of the refrigerator temperature. The junctions with Ni-Cr leads (solid symbols) all show a significantly higher resistance than the junctions with Cu-Au leads (open symbols). We can see also that the ZBR flattens out as the temperature is reduced, at a somewhat lower temperature for the junctions with the Ni-Cr leads than for the junctions with Cu-Au leads. In

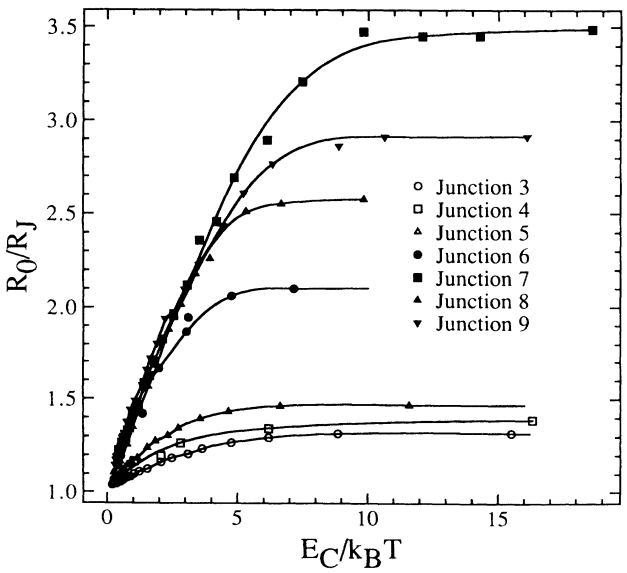

FIG. 7. Normalized zero-bias resistance vs temperature for seven small junctions. Open symbols are the Cu-Au leads, solid symbols for Ni-Cr leads. Lines are guides for the eye.

Table I, we summarize the parameters of nine junctions we have studied.

B. Diagnostic measurements

We made a number of attempts to explain the behavior of the ZBR as the temperature is lowered. We tested the possibility that the flattening was due to spurious high-frequency noise (radio- or microwave-frequency noise) by adding and removing the noise filters on the current and voltage leads at all three temperature stages (300 K, 4.2 K, and 20 mK). This had no effect on the low-temperature limit of the ZBR.

Another possibility is that the external circuit was still loading the junctions. We tested this possibility with one junction of each type by shorting out all but the first 4.5 mm of each lead with a layer of In (within the 4.5 mm section, the leads are too close together to be individually shorted with this technique). This procedure also had no effect on the ZBR, implying that the external circuit has been effectively isolated by the resistors, and that only the first few millimeters (at most) of the resistors affect the junctions.

As was mentioned earlier, there is the possibility of heating in the resistive leads, which could cause the flattening in the data. However, the design of the leads was intended to avoid problems caused by the hot-electron effect. Also it should be noted that the trend for the flattening to occur at a lower temperature for the higher resistivity Ni-Cr leads is inconsistent with this model. The fact that reducing the magnitude of the current modulation used for the differential measurements did not affect our results indicates that any heating caused by our measurement techniques should not be a factor, at least in the zero-bias limit. Finally, the magnitude of the spurious low-frequency noise also does not provide enough power to cause heating at the level needed to explain the data.

We conclude that the flattening of the ZBR at low temperature is most likely an intrinsic effect, and turn to a theoretical discussion of both this issue and the overall behavior of the I-V characteristics. We present two models which explicitly include the effects of the external

electromagnetic environment and appear to reproduce the main features seen in the data. One model was presented by us previously;[10] the other has been discussed by Nazarov[7] and developed further by other authors.[8,9] We also consider quantum fluctuations in the junctions themselves as a possible mechanism for flattening the ZBR as the temperature is reduced.

IV. THEORY OF ZERO-BIAS RESISTANCE

A. Quantum Langevin equation

Consider first the circuit, shown in Fig. 8(a), consisting of a small tunnel junction with capacitance C_J and tunnel resistance R_J in series with an ideal resistor R_L and a large stray capacitance $C_{\text{stray}} \gg C_J$. Let us place a charge Q on C_J at $T=0$: What happens as the charge Q is varied? For a charge $|Q| < e/2$ an electron must gain energy in order to tunnel across the junction barrier, and tunneling therefore occurs only for $|Q| > e/2$. If an electron takes a time τ to tunnel across the junction barrier and the circuit time constant $\tau_{RC} = R_L C_J \gg \tau$, then on the scale of τ the small junction in Fig. 8(a) *acts* as if it were isolated from the external circuit. Provided $\tau_{RC} \gg \tau$, the junction should therefore allow electrons to tunnel only for $|Q| > e/2$, and for $|Q| < e/2$ no tunneling should occur. A measurement of the I-V characteristic will therefore not reveal the presence of C_{stray}; however, something is missing from this picture, given the experimental evidence presented earlier.

How difficult is it to achieve the inequality $\tau_{RC} \gg \tau$? If we take[19] $\tau \approx 10^{-15}$ sec and $C_J = 10^{-15}$ F, then, even for a resistance R_L as low as 10 Ω, we find $\tau_{RC} = 10^{-14}$ sec, and the inequality is satisfied. However, if we consider the Heisenberg uncertainty relation $\Delta E\, \Delta t > \hbar$, the energy corresponding to the RC time constant is equivalent to a charge of about 20 e on C_J, so that the charge on the junction is not known very precisely.

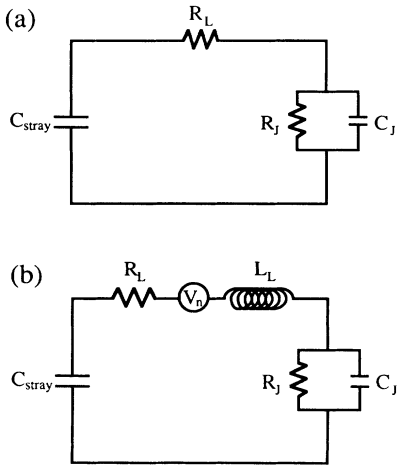

FIG. 8. (a) Circuit for small tunnel junction with resistance R_J and capacitance C_J connected through a large lead resistor R_L to low-impedance coaxial lines modeled by a large stray capacitance C_{stray}. (b) Circuit for a small tunnel junction, including lead resistance R_L and inductance L_L, and a large stray capacitance C_{stray}. Voltage noise source V_n is associated with R_L.

To complete this description, we must associate a voltage noise source V_n with R_L, as shown in Fig. 8(b), where we have also included the lead inductance L_L. The voltage source V_n drives current in the circuit loop, causing the charge Q to fluctuate over times much longer than τ. The classical equation of motion for the fluctuations $q(t)$ of the charge Q is given by

$$L_L \frac{d^2q}{dt^2} + R_L \frac{dq}{dt} + \left[\frac{1}{C_{\text{stray}}} + \frac{1}{C_J} \right] q = V_n(t) \, . \tag{2}$$

We Fourier transform Eq. (2) and solve for the spectral density of the charge fluctuations in terms of the spectral density of the voltage noise, $S_V(\omega)$:

$$S_q(\omega) = \frac{C_J^2}{(1-\omega^2/\omega_{LC}^2)^2 + (\omega/\omega_{RC})^2} S_V(\omega) \, . \tag{3}$$

Here we have defined the frequencies $\omega_{RC} = 1/R_L C_J$ and $\omega_{LC} = 1/\sqrt{L_L C_J}$, and neglected the stray capacitance with the assumption $C_{\text{stray}} \gg C_J$. To include quantum fluctuations we use the spectral distribution of voltage noise given by the full Johnson-Nyquist formula:[20]

$$S_V(\omega) = \frac{\hbar\omega R_L}{\pi} \coth(\hbar\omega/2k_B T) \, . \tag{4}$$

This expression reduces to $S_V(\omega) = 2k_B T R_L/\pi$ in the limit $\hbar\omega \ll k_B T$ and to $S_V(\omega) = \hbar\omega R_L/\pi$ for $\hbar\omega \gg k_B T$. Even at $T=0$ there are significant voltage fluctuations caused by the resistor.

Using the Wiener-Khinchine theorem, we can write the instantaneous charge fluctuation $\langle q^2(t) \rangle$ in terms of the frequency-domain fluctuations,

$$\langle q^2(t) \rangle = \int_0^\infty S_q(\omega) d\omega \, . \tag{5}$$

We can carry out the integral in Eq. (5) analytically in two limits; for $\hbar\omega \ll k_B T$ we obtain the result expected from equipartition of energy, $\langle q^2 \rangle / 2C_J = k_B T/2$. For $\hbar\omega \gg k_B T$, for $\alpha = \omega_{LC}/\omega_{RC} < 2$, we find

$$\frac{\langle q^2(t) \rangle}{2C_J} = \frac{\hbar\omega_{LC}}{2\pi} \frac{1}{\sqrt{4-\alpha^2}} \left[\frac{\pi}{2} - \tan^{-1} \left[\frac{\alpha^2-2}{\alpha\sqrt{4-\alpha^2}} \right] \right] . \tag{6}$$

For very small α, Eq. (6) reduces to $\langle q^2(t) \rangle / 2C = \hbar\omega_{LC}/4$, as expected for a simple harmonic oscillator with no dissipation. For $\hbar\omega \gg k_B T$ and $\alpha > 2$, we find

$$\frac{\langle q^2(t) \rangle}{2C_J} = \frac{\hbar\omega_{LC}}{4\pi} \frac{1}{\sqrt{4-\alpha^2}} \ln \left[\frac{\alpha^2-2+\alpha\sqrt{\alpha^2-4}}{\alpha^2-2-\alpha\sqrt{\alpha^2-4}} \right] . \tag{7}$$

In the limit of very large R_L we find that $\langle q^2 \rangle / 2C = (\hbar\omega_{RC}/\pi) \ln\alpha$, which varies as $1/R_L$ and has only a logarithmic dependence on L_L. In Fig. 9(a) we plot $\langle q^2 \rangle / e^2$ versus R_L for $L_L = 4.5$ nH and $C_J = 4.5$ fF at $T=0$. We have chosen the values of C_J and L_L to be representative of the capacitances of junctions 5 and 7

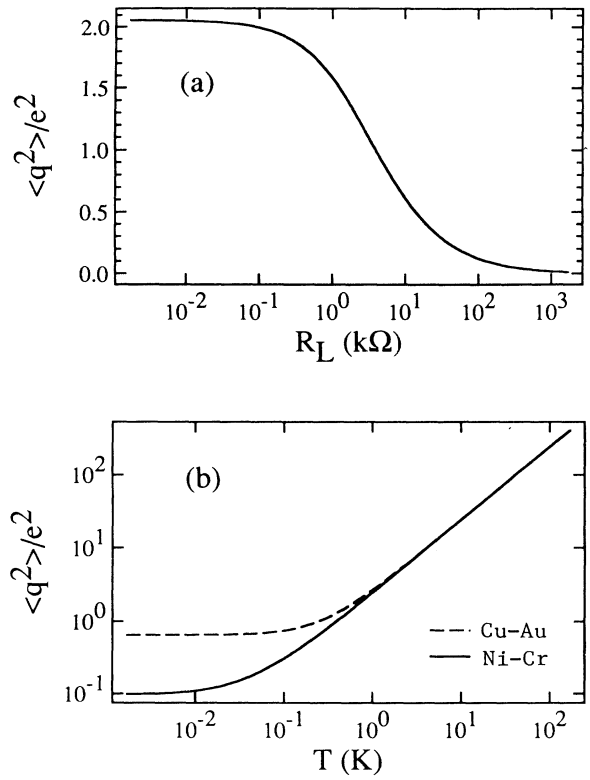

FIG. 9. (a) Dependence of $\langle q^2\rangle/e^2$ on R_L for junction capacitance $C_J=4.5$ fF, lead inductance $L_L=4.5$ nH, calculated using the quantum Langevin theory at $T=0$. (b) Plot of temperature dependence of $\langle q^2\rangle/e^2$, calculated from the quantum Langevin theory, for both Cu-Au and Ni-Cr leads; see text for circuit parameters.

and the inductance of the first 4.5 mm of the resistive leads, respectively. In Fig. 9(b) we display the temperature dependence of $\langle q^2\rangle/e^2$ for $L_L=4.5$ nH, $C_J=4.5$ fF, and $R_L=9.0$ and 130 kΩ, the latter being the resistance for the first 4.5 mm of the Cu-Au and Ni-Cr leads, respectively.

The value of $\langle q^2\rangle$ is the spread of the distribution $P(q)$, which describes the probability of having a charge fluctuation of size q on the small junction capacitor C_J; previously we assumed the probability distribution to be $P(q)=\delta(q)$. The spread in the values of q arises, in general, from both thermal and quantum fluctuations. In the limit of zero temperature, the probability distribution is the square of the wave function (i.e., the probability amplitude) of the variable q.

To accommodate the spread in the values of q in the calculation of the current-voltage characteristic, we assume that the effective tunneling rate $\langle\Gamma(Q)\rangle$ of electrons is the tunneling rate $\Gamma(Q)$ in the absence of fluctuations, convolved with the probability $P(q)$ of a given size fluctuation q. As the fluctuations are concentrated at frequencies much below the inverse electron tunneling time $1/\tau$, this should be a reasonable approximation. The resulting expression is

$$\langle\Gamma(Q)\rangle=\int_{-\infty}^{\infty}\Gamma(Q+q)P(q)dq\ . \tag{8}$$

An expression for $\Gamma(Q)$ can be derived analytically:[21]

$$\Gamma^{\pm}(Q)=-\frac{e/2\pm Q}{eR_JC_J}[\exp(\Delta E^{\pm}/k_BT)-1]^{-1}\ , \tag{9}$$

where $\Gamma^{\pm}$ is the rate for Q to go to $Q\pm e$. Assuming the probability distribution $P(q)$ to be Gaussian,

$$P(q)=\frac{1}{\sqrt{2\pi\langle q^2\rangle}}\exp\left[-\frac{q^2}{2\langle q^2\rangle}\right]\ . \tag{10}$$

We can carry out the convolution of Eq. (8) analytically at $T=0$ to obtain

$$\langle\Gamma^{\pm}\rangle=-\frac{e/2\pm Q}{2eR_JC_J}\mathrm{erfc}\left[\frac{e/2\pm Q}{\sqrt{2\langle q^2\rangle}}\right]+\frac{1}{eR_JC_J}\sqrt{\langle q^2\rangle/2\pi}\exp\left[-\frac{(e/2\pm Q)^2}{2\langle q^2\rangle}\right]\ . \tag{11}$$

In Fig. 10 we plot $\langle\Gamma(Q)\rangle$ and $\Gamma(Q)$ at $T=0$ for $\langle q^2\rangle=0.65$ and 0.098 e^2 (the values for the Cu-Au and Ni-Cr leads) to show the smearing of the Coulomb gap due to the uncertainty in the value of Q. Note that at large values of Q, the two rates are identical; the smearing only occurs for values of Q within $\sqrt{\langle q^2\rangle}$ of $\pm e/2$.

Using the above discussion, we can explain the main experimental features of the data in terms of this simple model: The smearing of the Coulomb gap at low-bias voltages is caused by fluctuations in the leads, becoming less apparent as the fluctuations are reduced in magnitude by increasing the value of the lead resistance, or by reducing the temperature. We furthermore see that the zero-temperature limit of the current-voltage characteristic can be explained by the inclusion of the zero-point quantum fluctuations in the leads. To make a more quan-

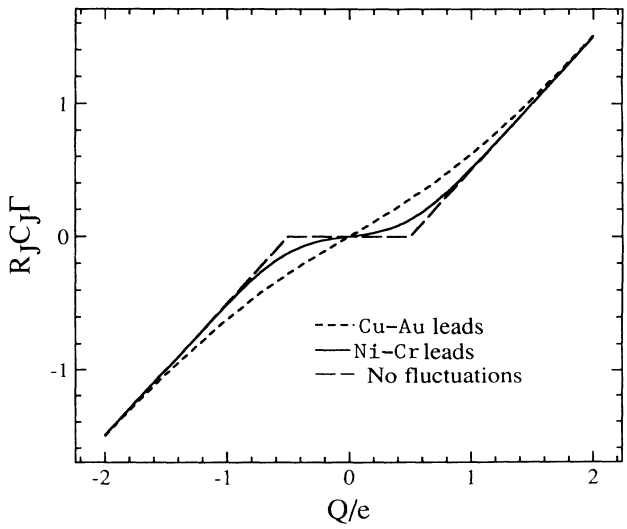

FIG. 10. $T=0$ tunneling rate Γ, normalized to high-bias rate $1/R_JC_J$ as predicted by the quantum Langevin theory vs charge Q/e. The dotted curve is for Cu-Au leads and the solid curve is for Ni-Cr leads, with circuit parameters given in text. The dashed curve is tunneling rate in the absence of fluctuations.

titative comparison between them and experiment, we have to choose parameters for our circuit model; this simple quantum Langevin approach unfortunately does not yield solutions for the more complete resistive transmission line model of the leads. To make a reasonable approximation to the actual circuit, we choose to include only the first 4.5 mm of each lead, and treat the estimated values of the resistive transmission line as lumped circuit elements choosing the total inductance to be 4.5 nH, and the resistance to be 9 kΩ for the Cu-Au leads and 130 kΩ for the Ni-Cr leads. We estimated the junction capacitance from the high-current limit of the Coulomb offset for the two junctions; according to the theory sketched out above, this procedure should be correct even in the presence of fluctuations.

One part of the experimental situation which we have thus far ignored in our use of a current bias rather than the voltage bias used in our calculations of the tunneling rates The situation is complicated by the presence of the stray capacitance in the circuit; in Fig. 11(a) we show the model circuit with a current bias element $I_{\rm bias}$ connected across the stray capacitance $C_{\rm stray}$. The junction is modeled as a capacitance in parallel with a current source $I_J(t)$ that transfers single electrons across the junction. The junction follows a charging-discharging sequence, and on average the time between discharging events is given by $\Delta t = e/I_{\rm bias}$. The junction voltage follows two distinct patterns, depending on whether the charging time $\tau = R_L C_J$ is much larger or much smaller than Δt (the inductance L_L is too small to have a noticeable effect). In the limit $\tau \ll \Delta t$, shown in Fig. 11(b), the voltage recovers rapidly after an electron has tunneled and spends most of its time before the next tunneling event near the average value $\langle V_J \rangle$. This voltage then satisfies the relation

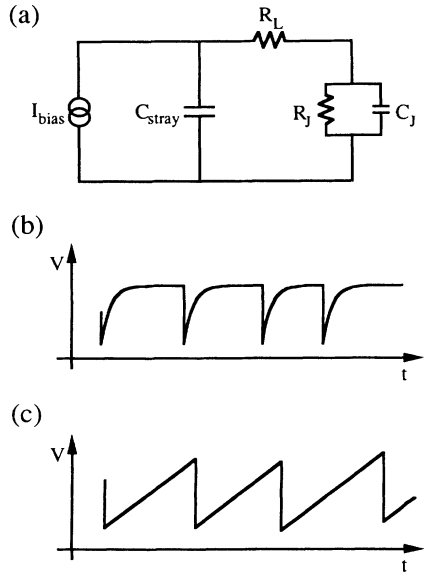

FIG. 11. (a) Model circuit for nearly current-biased measurement. Charging-discharging sequence for bias current $I_{\rm bias}$ with (b) $R_L C_J \ll e/I_{\rm bias}$ and (c) $R_L C_J \gg e/I_{\rm bias}$.

$$\langle \Gamma(\langle V_J \rangle) \rangle = I_{\rm bias}/e \ . \tag{12}$$

In other words, in this limit the junction is effectively voltage biased, and the I-V characteristic is given by Eq. (12), where $\langle \Gamma(V) \rangle$ is the result of Eq. (11).

In the opposite limit $\tau \gg \Delta t$, shown in Fig. 11(c), the junction voltage ramps up linearly and the junction is effectively current biased. One must calculate the I-V characteristic numerically by following the charging-discharging sequence in time. To calculate the I-V characteristic without using an inordinate amount of computation time, we developed an approximate method, which, for the experimental data, is estimated to have errors of at most 3%. In the approximation, we fix the time between tunneling events at $\Delta t = e/I_{\rm bias}$, rather than allow this time to fluctuate because of the stochastic nature of electron tunneling. The current source $I_J(t)$ then provides a regular series of δ functions, with amplitude $-e$ separated in time by Δt. We calculate the voltage $V(t)$ by solving the circuit equations for Fig. 11(a) at a fixed $I_{\rm bias}$, finding the mean voltage $\langle V(t) \rangle$ by solving the equation

$$\frac{1}{\Delta t} \int_t^{t+\Delta t} \langle \Gamma[V(t)] \rangle dt = I_{\rm bias}/e \ . \tag{13}$$

Self-consistent solutions of Eq. (13) as a function of $I_{\rm bias}$ yield the I-V characteristic.

In Fig. 12 we plot the comparison of the theory at $T=0$ and the experimental data. The data for the Cu-Au leads are in reasonable agreement at low bias and less

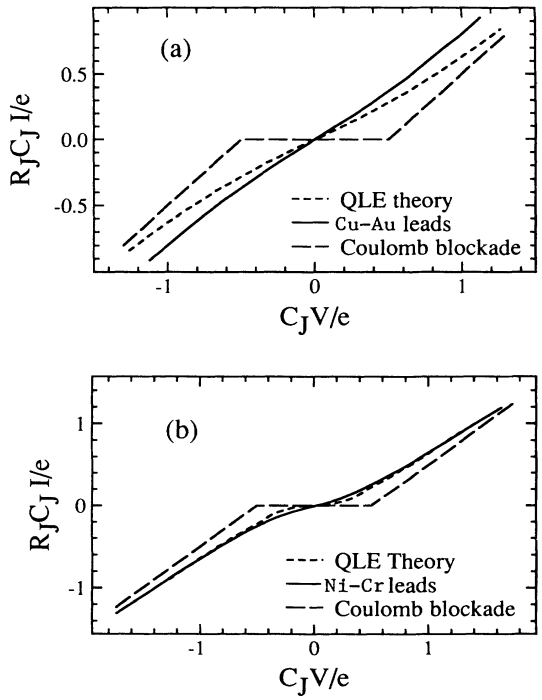

FIG. 12. Comparison of the quantum Langevin theory with experimental I-V characteristics: (a) is junction 5 with Cu-Au leads and (b) is junction 7 with Ni-Cr leads. The solid dots are quantum Langevin equation (QLE) predictions at $T=0$, and the dashed line is the predicted voltage-biased Coulomb blockade.

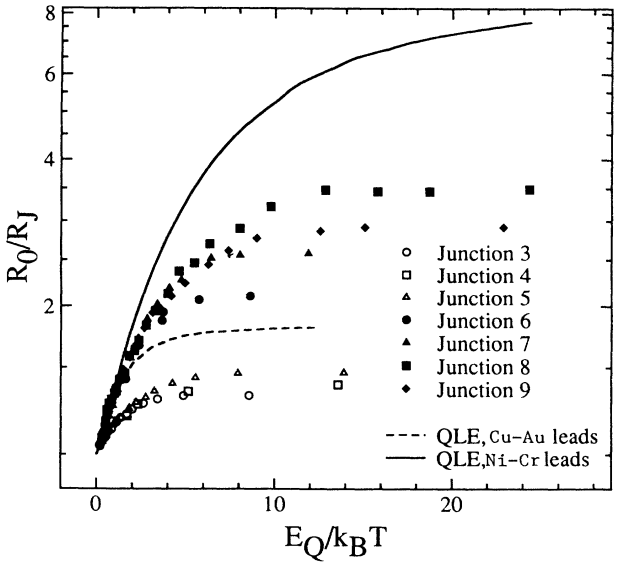

FIG. 13. Zero-bias resistance predicted by the quantum Langevin equation (lines), compared with the experimental results (symbols) for seven junctions. Open symbols and dashed line are Cu-Au leads, solid symbols and solid line are Ni-Cr leads.

good agreement at high bias, while the data for the Ni-Cr leads show reasonable agreement over the entire range of displayed bias currents. In Fig. 13 we have plotted the calculated temperature dependence of the zero-bias resistance together with the experimental results. The experiment and theory are seen to have the same approximate shape, with roughly the same rate of increase of resistance with decreasing temperature, and to flatten out at roughly the same value of resistance. Note that, by fitting the parameters, in particular, the length of lead used in the model circuit, we could obtain a much better agreement for the temperature dependence of the ZBR. However, the heuristic nature of this model is such that we wish only to show that the general behavior can be predicted; we do not claim that this model includes all relevant details. A discussion of the more rigorous theory follows.

B. Phase-correlation theory

Several authors have published different versions of an alternative theory to the quantum Langevin theory presented above.[7–9] We here summarize the version described by Devoret *et al.*[8]

The essence of the approach is to treat both the junction capacitor and its environment as a single quantum system. The tunneling in the junction is then added as a perturbative term in the Hamiltonian, coupled to the electromagnetic system. In this way the energy of the entire circuit is included when one calculates the tunneling rate of electrons across the junction; this is in contrast to the simplest theory where the external circuit is ignored and only the charging energy of the junction capacitance is considered. Taking this approach, Devoret *et al.* develop an expression for the phase-correlation function $J(t)$ given by

$$J(t)=\langle[\delta(t)-\delta(0)]\delta(0)\rangle\ , \tag{14}$$

where

$$\delta(t)=\int_{-\infty}^{t}V(t')dt' \tag{15}$$

is the phase variable across the normal junction. The phase-correlation function is given by

$$J(t)=\int_0^\infty\frac{d\omega}{\omega}\frac{\mathrm{Re}Z_t(\omega)}{(R_K/2)}\times\left[\coth\left[\frac{\beta\hbar\omega}{2}\right][\cos(\omega t)-1]-i\sin(\omega t)\right]\ , \tag{16}$$

where we define $\beta=1/k_BT$, the total impedance function $Z_t(\omega)$ is given by $Z_t^{-1}(\omega)=i\omega C+Z^{-1}(\omega)$, and the normal-metal resistance quantum is $R_K/2=h/2e^2=12.91\ \mathrm{k\Omega}$. Knowledge of the phase-correlation function allows one to calculate the probability $P(E)$ that an electron will lose energy E in the circuit through the expression

$$P(E)=\frac{1}{2\pi\hbar}\int_{-\infty}^{\infty}dt\,\exp[J(t)+iEt/\hbar]\ . \tag{17}$$

When the impedance of the environment approaches the infinite limit, $P(E)$ approaches a δ function, and the electron cannot exchange energy with the environment; the junction becomes isolated from its environment as we described earlier. For a finite impedance, $P(E)$ is distributed, and from this the tunneling rate Γ at a voltage $V=Q/C$ can be calculated from the expression

$$\Gamma(V)=\frac{1}{e^2R_J}\int_{-\infty}^{\infty}dE\,E\frac{1-\exp(-\beta eV)}{1-\exp(-\beta E)}P(eV-E) \tag{18}$$

for a junction with tunnel resistance R_J. Because the tunneling is included only as a perturbation, this derivation assumes that quantum fluctuations in the junction itself can be neglected, i.e., that R_J is much larger than the resistance quantum $R_K/2$; it also assumes $\mathrm{Re}[Z(\omega)]\ll R_J$. An alternative formulation of this theory appears in a paper by Ingold and Grabert.[22]

Equation (18) gives the voltage-biased tunneling rate $\Gamma(V)$; just as for the case of the quantum Langevin equation discussed in Sec. IV A, we have to account for the actual biasing circuit used in the experiment. We have chosen to use the same approximate method described in that section, using a fixed time $\Delta t=e/I_{\mathrm{bias}}$ between tunneling events. However, we replace the simple RLC circuit with the impedance $Z_t(\omega)$ inferred from the measured static resistance of the leads, and the numerically calculated values of the capacitance and inductance of the leads, as discussed in Sec. II A.

One would, of course, prefer to use an impedance $Z(\omega)$ obtained from a direct measurement. However the relevant frequencies involved in the phase-correlation

function, Eq. (16), are of the order of $e^2/2Ch \approx 10^{10}$ Hz, a range in which such measurements are difficult. The circuit in question involves the thin-film leads, which can be accurately modeled as a resistive transmission line, connected to the low-impedance coaxial measurement leads which present a more complicated impedance. However, the impedance of the thin-film leads is large enough (of the order of a few kΩ) even at the relevant frequencies to isolate the junction from the rich environment of the coaxial leads, and we thus expect the simple impedance model to be adequate.

Figure 14 shows the calculated I-V characteristics compared with those for junctions 5 and 7, taken at $T=20$ mK. In Fig. 15 we compare the differential resistance predictions with the experiment; the temperatures for the theory are as in Fig. 14. We see that, in both cases, the high-current I-V characteristic agrees fairly well, but at lower currents the I-V shows less curvature than the theory predicts. This is borne out better in the differential resistance traces, where we find the predicted ZBR is somewhat higher than measured, and the differential resistance curve is broader in the measurement than in the theory, especially in the case of Cu-Au resistors.

A possible source of error in the calculated curves involves the choice of the parameters for the transmission line, in particular, the value of the capacitance per unit length. We calculate this capacitance numerically by allowing charge to flow onto a model section of the transmission line until the potential is uniform; the ratio of the potential to the charge gives the capacitance. This method, when applied to simple geometries, gives the correct result for the capacitance to within 20%. Variations in the value of C_L of this magnitude for the calcula-

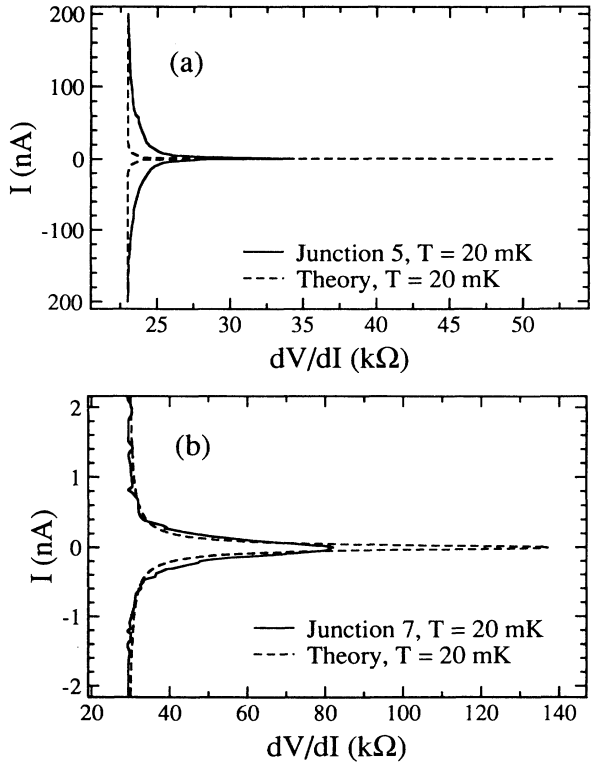

FIG. 15. Comparison of the theory of Devoret *et al.* (Ref. 20) with experimental dV/dI measurements at $T=20$ mK: (a) junction 5 and (b) junction 7.

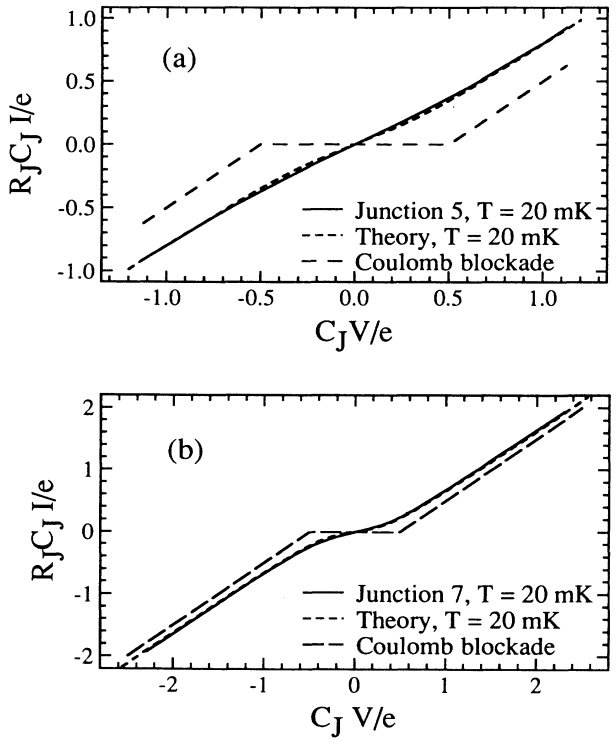

FIG. 14. Comparison of theory of Devoret *et al.* (Ref. 20) with experimental I-V characteristics; (a) is junction 5 and (b) is junction 7. Both the data, shown by solid lines, and the theory curves, shown by dashed lines, are at $T=20$ mK. The voltage-biased Coulomb blockade is also shown.

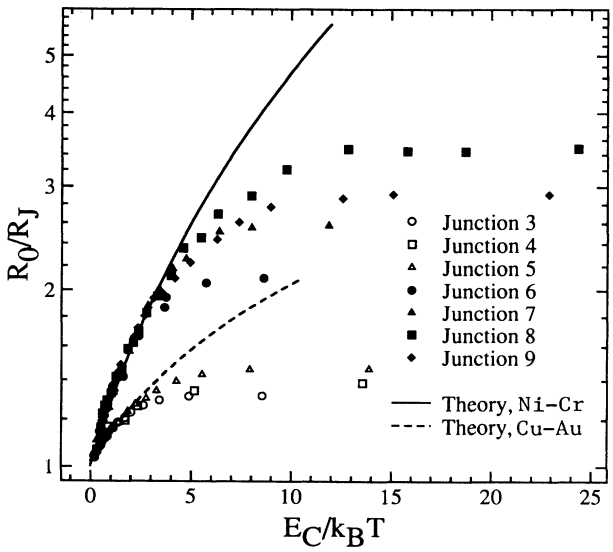

FIG. 16. Zero-bias resistance for seven junctions compared with theory of Devoret *et al.* (Ref. 20), with circuit parameters for Cu-Au leads (dashed line, open symbols) and Ni-Cr leads (solid line, solid symbols).

tions of Fig. 14 do not give noticeable differences in the curves. Larger variations in the value of C_L result in changes in the high-bias offset of these curves, with little change in the low-current bias region. The agreement between the calculated and measured curves in the high-bias region implies that our estimated value of C_L is not unreasonable.

The temperature dependence of the zero-bias resistance for both types of lead material is compared with the theory in Fig. 16; the data have been plotted as a function of $E_Q/k_BT=e^2/(2C_Jk_BT)$. A detailed comparison requires more precisely known values of the junction capacitance C_J than those given in Table I; to make the comparison of Fig. 16, we have adjusted the values of C_J slightly to give agreement at high temperatures. Values of C_J for the Cu-Au leads were adjusted upward and those for the Ni-Cr leads downward, within the estimated uncertainties from the I-V measurements. In general, the comparison at high temperatures is quite good, but the experimental results flatten off as the temperature is lowered while the theoretical predictions continue to increase. As discussed earlier, several attempts were made to explain the zero-bias behavior in terms of spurious noise and heating, none of which were shown to have any effect on the measurements. As it stands, therefore, there is no good explanation for this discrepancy.

C. Quantum fluctuations in the junctions

There is an interesting trend observed in the experimental ZBR data: the junctions with smaller R_J are seen to flatten off at smaller values of R_0/R_J, where R_0 is the zero-bias differential resistance, than those with larger R_J. This trend could be due to quantum fluctuations in the junctions themselves. This question is discussed in a paper by Brown and Šimánek,[23] who calculate the ZBR of a single small junction as a function of temperature and junction resistance. However, these authors do not include the effect of the environment, and treat the junction resistance as an Ohmic shunt. An experiment investigating the effects of finite junction resistance in devices involving multiple series-connected small junctions[6] appears to confirm the calculation. In Fig. 17 we show the predicted ZBR of a single junction versus R_J, normalized to the resistance quantum $R_K/2=h/2e^2$, at the two temperatures $E_Q/k_BT=10$ and $E_Q/k_BT=7.5$. There is clearly a strong dependence of the ZBR on tunneling resistance, and the general trends are reproduced in the experimental data obtained with Ni-Cr shunts. Thus, it seems entirely possible that a complete theory for the ZBR requires one to combine the effects of both the finite tunnel-junction resistance and the environment.

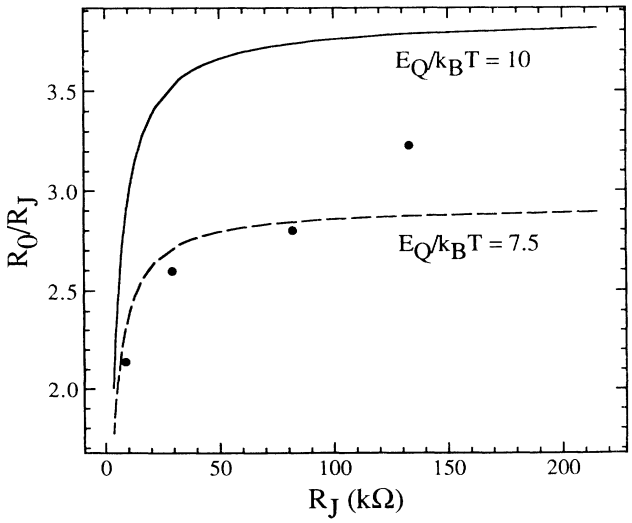

FIG. 17. Zero-bias resistance R_0/R_J calculated from theory of Brown and Šimánek for $E_Q/k_BT=10$ and 7.5. Also shown are zero-bias resistance data for the junctions with Ni-Cr leads at $E_Q/k_BT=10$.

V. SUMMARY

We have described the results of measurements on a series of single, low-capacitance tunnel junctions connected to thin-film resistors with resistances of either about 2 or 30 kΩ/μm. The I-V characteristics of the junctions are strongly influenced by the impedance presented by these leads; in particular, the Coulomb blockade is much more clearly visible for the high-resistance leads than for the low-resistance leads. The zero-bias resistance R_0 of the junctions increases as the temperature is lowered, flattening off at the lowest temperatures. We have demonstrated that this flattening could not be explained by Joule heating in the junctions and the leads, nor by the influence of extraneous noise sources.

In an attempt to obtain a heuristic understanding of the effects of the leads, we developed a simple model based on the quantum Langevin equation. In this picture, Nyquist noise in the leads produces fluctuations in the charge on the junction, smearing out the current-voltage characteristics even at $T=0$, where zero-point fluctuations remain. This model provides a qualitatively correct description of our data. In particular, the Coulomb blockade is predicted to be much less smeared out in the case of high-resistance leads than in the case of low-resistance leads, although the quantitative agreement between theory and experiment is much better for the former than for the latter. The model also predicts the flattening of R_0 as $T\rightarrow 0$, although the predicted values of R_0/R_J are too high in both cases. However, this discrepancy may well be explained by our inexact knowledge of the values of the lead resistances.

We also compared our data with the phase-correlation theory, which treats the entire circuit as a single quantum system, and includes a more accurate, transmission-line model for the leads. This model yields a better prediction of the I-V characteristics for both high- and low-resistance leads, although an examination of the differential resistance shows that the predicted zero-bias resistance at the lowest temperatures is roughly 50% higher than the data in each case. In contrast to the data and the quantum Langevin model, the phase-correlation theory predicts that R_0/R_J continues to increase as the temperature is lowered. This disagreement suggests that quantum fluctuations in the junction, which are not in-

cluded in the phase-correlation theory, may indeed play a role at lower temperatures. Further theoretical work will be required to test this hypothesis quantitatively.

ACKNOWLEDGMENTS

We thank M. Devoret, U. Eckern, D. Esteve, H. Grabert, H. Mooij, Y. Nazarov, and G. Schön for helpful discussions. We thank the staff of the Microfabrication Facility of the Electrical Engineering and Computer Science Department for their expert assistance, and T. Van Duzer for the use of his scanning electron microscope. One of us (A.N.C.) acknowledges partial support by IBM. This work was supported by the Director, Office of Energy Research, Office of Basic Energy Sciences, Materials Sciences Division of the U.S. Department of Energy under Contract No. DE-AC03-76SF00098.

[1]See, e.g., D. V. Averin and K. K. Likharev, J. Low Temp. Phys. **62**, 345 (1986).
[2]T. A. Fulton and G. J. Dolan, Phys. Rev. Lett. **59**, 109 (1987).
[3]L. S. Kuzmin, P. Delsing, T. Claeson, and K. K. Likharev, Phys. Rev. Lett. **62**, 2539 (1989).
[4]P. Delsing, K. K. Likharev, L. S. Kuzmin, and T. Claeson, Phys. Rev. Lett. **63**, 1180 (1989).
[5]P. Delsing, K. K. Likharev, L. S. Kuzmin, and T. Claeson, Phys. Rev. Lett. **63**, 1861 (1989).
[6]L. J. Geerligs, V. F. Anderegg, C. A. van der Jeugd, J. Romijn, and J. E. Mooij, Europhys. Lett. **10**, 79 (1989).
[7]Yu. V. Nazarov, Zh. Eksp. Teor. Fiz. **95**, 975 (1989).
[8]M. Devoret, D. Esteve, H. Grabert, G.-L. Ingold, H. Pothier, and C. Urbina, Phys. Rev. Lett. **64**, 1824 (1990).
[9]S. Girvin, L. I. Glazman, M. Jonson, D. R. Penn, and M. D. Stiles, Phys. Rev. Lett. **64**, 3183 (1990).
[10]A. N. Cleland, J. M. Schmidt, and J. Clarke, Phys. Rev. Lett. **64**, 1565 (1990).
[11]D. V. Averin and K. K. Likharev, J. Low Temp. Phys. **59**, 347 (1985).
[12]A. N. Cleland, Ph.D. thesis, University of California at Berkeley, 1991.
[13]J. M. Jaycox and M. B. Ketchen, IEEE Trans. Mag. **MAG-17**, 400 (1981).
[14]F. C. Wellstood, C. Urbina, and J. Clarke, Appl. Phys. Lett. **54**, 2599 (1989).
[15]G. J. Dolan, Appl. Phys. Lett. **31**, 337 (1977).
[16]R. E. Howard, E. L. Hu, L. D. Jackel, L. A. Fetter, and R. H. Bosworth, Appl. Phys. Lett. **35**, 879 (1979).
[17]J. M. Martinis and R. L. Kautz, Phys. Rev. Lett. **63**, 1507 (1989).
[18]J. M. Martinis, M. H. Devoret, and J. Clarke, Phys. Rev. B **35**, 4682 (1987).
[19]M. Büttiker and R. Landauer, IBM J. Res. Dev. **30**, 451 (1986).
[20]J. B. Johnson, Phys. Rev. **32**, 97 (1928); H. Nyquist, *ibid.* **32**, 110 (1928).
[21]U. Geigenmüller and G. Schön, Physica (Amsterdam) **152B**, 186 (1988).
[22]G.-L. Ingold and H. Grabert, Europhys. Lett. **14**, 371 (1991).
[23]R. Brown and E. Šimánek, Phys. Rev. B **34**, 2957 (1986).